Density-functional based determination of intermolecular charge transfer properties for large-scale morphologies

Björn Baumeier,*[a] James Kirkpatrick[b] and Denis Andrienko[a]

Theoretical studies of charge transport in organic conducting systems pose a unique challenge since they must describe both extremely short-ranged and fast processes (charge tunneling) and extremely long-ranged and slow ones (molecular ordering). The description of the mobility of electrons and holes in the hopping regime relies on the determination of intermolecular hopping rates in large-scale morphologies. Using Marcus theory these rates can be calculated from intermolecular transfer integrals and on-site energies. Here we present a detailed computational study on the accuracy and efficiency of density-functional theory based approaches to the determination of intermolecular transfer integrals. First, it is demonstrated how these can be obtained from quantum-chemistry calculations by forming the expectation value of a dimer Fock operator with frontier orbitals of two neighboring monomers based on a projective approach. We then consider the prototypical example of one pair out of a larger morphology of tris(8-hydroxyquinolinato)aluminium (Alq_3) and study the influence of computational parameters, e.g. the choice of basis sets, exchange–correlation functional, and convergence criteria, on the calculated transfer integrals. The respective results are compared in order to derive an optimal strategy for future simulations based on the full morphology.

I. Introduction

The rapidly growing field of organic semiconductors is driven mainly by two factors: (i) the possibility to combine electronic properties of semiconductors with mechanical properties of soft condensed matter, which has clear advantages for large-scale material processing, and (ii) the ability to synthetically control both electronic and self-assembly properties. In spite of recent advancements, the main limiting factors of state-of-the-art materials is their stability and low charge carrier mobility. Hence, optimization of charge transport is essential in order to improve efficiency of devices. In this situation, computer simulation can help to pre-screen available compounds by formulating appropriate structure–processing property (in this case charge mobility) relationships or even help to rationally design organic semiconductors.[1–5]

Several techniques have been used to describe charge transport in organic semiconductors. For ordered crystals, the Drude model is often used, with the charge mobility determined from the mean free relaxation time of the band states and effective mass of charge carriers.[6–9] The simple band-like picture can be adjusted to take into account electron–phonon coupling.[10–13] If the wavefunction is no longer completely delocalized and charge transport becomes diffusion-limited by thermal disorder, the semi-classical dynamics model based on a Hamiltonian with interacting electronic and nuclear degrees of freedom can be used.[14–16]

If charge transport occurs in the non-adiabatic regime or is strongly limited by trapping, a common approach is to solve rate equations for charge hopping. In the Gaussian disorder model, the distributions on the rate parameters[17] are chosen empirically. Another approach is to explicitly compute charge transfer parameters for a given arrangement of molecules using temperature-activated non-adiabatic transfer in the high-temperature regime given by Marcus theory[18,19]

$$\omega_{nm} = \frac{t_{nm}^2}{\hbar} \sqrt{\frac{\pi}{\lambda k_B T}} \exp\left[-\frac{(\Delta G_{nm} - \lambda)^2}{4 k_B T \lambda} \right], \qquad (1)$$

where λ is the reorganization energy and $\Delta G_{nm} = \varepsilon_n - \varepsilon_m$ is the free energy difference between initial and final states. The latter approach is technically more complex but has the advantage of allowing one to relate charge transport properties directly to morphology.[3–5,20–24] The morphology itself can be determined by using molecular dynamics or Monte Carlo simulations.

In all of the models used, it is useful to keep in mind an effective Hamiltonian of the type

$$\hat{H} = \sum_m \varepsilon_m \hat{a}_m^+ \hat{a}_m + \sum_{m \neq n} (t_{mn} \hat{a}_m^+ \hat{a}_n + \text{c.c.}), \qquad (2)$$

where $\hat{a}_m^+$ and $\hat{a}_m$ are the creation and annihilation operators for a charge carrier located at the molecular site m. The electron site energy is given by ε_m, while t_{mn} is the transfer integral between two sites m and n. The distribution in ε_m describes the density of states whereas t_{mn} sets a timescale for charge tunneling.

In the framework of the frozen-core approximation, the usual choice for the basis set representing the electron states from eqn (2) are the frontier orbitals: the highest occupied

[a] Max Planck Institute for Polymer Research, Ackermannweg 10, D-55128 Mainz, Germany. E-mail: baumeier@mpip-mainz.mpg.de
[b] Centre for Electronic Materials and Devices, Department of Physics, Imperial College London, London SW7 2BW, United Kingdom

molecular orbital (HOMO) if we are talking of hole transport, and the lowest unoccupied molecular orbital (LUMO) if we are talking about electron transfer. The off-diagonal elements of eqn (2) are the same as the transfer integrals t_{mn} for a pair of molecules, so long as we ignore the possibility that neighboring molecules affect the frontier orbitals by polarization. The situation is more complicated for the site energies ε_m. We can imagine several different contributions to energetic disorder: (i) due to change of a molecular conformation, (ii) due to electrostatic and (iii) polarization contributions.

Conformational disorder refers to the fact that molecules often find themselves frozen in positions which do not correspond to their energetic minimum. For example, in a conjugated polymer torsional disorder can lead to a distribution in site-energies.[25] One of the molecules discussed here, Alq$_3$, has this sort of "soft" degrees of freedom which affect the position of its HOMO and LUMO levels. Conformational disorder can be analyzed by performing calculations on isolated molecules in the deformed geometries provided by molecular dynamics. It is important to be careful to only include those geometry fluctuations which are slow with respect to charge transport (e.g. dihedral angles).

Electrostatic disorder arises because the electric field distribution from a charge is far from isotropic. Therefore molecules in different positions in the lattice have different electrostatic energies. The importance of electrostatic disorder has been known for a long time and is best evidenced in the strong correlation between energetic disorder and dipole moment for polar molecules diluted in an inert polymer matrix.[26] Since electrostatic interactions are pairwise-additive, the energy of a whole assembly of molecules can easily be derived from computations on pairs. It is, however, not feasible to perform accurate first-principles calculations on all molecular pairs needed to evaluate the electrostatic contribution to the energetic disorder. Instead, partial charges distributed on each molecule are often used for this purpose.[27,28]

Polarization itself can lead to disorder because the polarizability of most conjugated molecules is highly anisotropic. This, however, is by far the least discussed in the literature source of disorder.[28,29] The polarization contribution is not pairwise-additive and cannot be deduced from the calculations on the pairs of molecules.

Naturally, we can ask ourselves, what information that is useful for large-scale simulations can be obtained from a calculation on a pair of molecules? Evidently, the transfer integrals will directly be related to the transfer integrals between those two molecules. The site-energies will however be specific to the *pair configuration* and will include all three disorder effects mentioned above for this specific geometry. Hence, in general, it will not be at all easy to extract site energy information for a whole simulation box from many calculations on pairs. The practical solution to this is to use transfer integrals for pairs of molecules and site energies from calculations of monomers with the fast molecular degrees of freedom constrained to their optimized values. This will take into account energetic disorder due to soft degrees of freedom, such as dihedral angles. Finally, electrostatic and polarization

contributions can be estimated from partial charges or polarizable force-field calculations.

In what follows, we assess the performance of several schemes designed for efficient calculation of intermolecular transfer integrals and site energies for *pairs* of molecules.

Semiempirical approaches such as Zerner's Intermediate Neglect of Differential Overlap (ZINDO) have been quite well established in application to hydrocarbon compounds, e.g. for different mesophases of discotic liquid crystals such as perylene and hexabenzocoronene derivatives.[20,21] However, for metal-coordinated molecules, for instance, the ZINDO parametrization is inappropriate and as a consequence wrongly predicts the localization of molecular frontier orbitals which directly relates to incorrect values for the charge transport properties. This is the case, e.g. for tris(8-hydroxy-quinolinato)aluminium (Alq$_3$), a common organic semiconductor, which in experiment exhibits a higher mobility for electrons than for holes.[30] The first organic light-emitting diodes were based on Alq$_3$, and subsequently this compound has become a prototypical system in organic electronics.[31] To understand the relation between charge dynamics and morphology in such a system, it is essential to determine intermolecular transfer integrals and site-energies in a qualitatively and quantitatively reliable fashion.

Calculating the respective properties from first-principles density-functional theory (DFT) is far more elaborate and computationally demanding than semiempirical approaches, but promises to work well in the cases mentioned above in which ZINDO fails. Several approaches for the derivation of charge transport parameters have been discussed in the literature. Since the interaction of two monomers in a dimer configuration leads to a splitting of the HOMO level of the dimer, it is quite common practice (see e.g. ref. 2, 32 and 33) to relate the transfer integral to half of the difference of HOMO and HOMO − 1 levels resulting from a closed-shell configuration of the dimer. However, Valeev and coworkers[32] pointed out that polarization effects can have a decisive influence on the energy splitting, which alone is therefore not a good measure for the transfer integral. Based on this procedure, Huang and Kertesz[34] studied the convergence of transfer integrals of a π-stacked ethylene dimer with respect to the basis set of DFT calculations and identified the effects of diffuse and polarization functions on the results. The same authors later investigated the effects of different choices for the exchange–correlation functional[33] and found that, while not negligible, the differences are relatively small. In a study of carrier transport in crystalline silole-based compounds, Yin et al.[35] determined the electronic coupling between initial and final states by setting up the dimer Fock operator using unperturbed monomer orbitals and forming the Fock matrix elements with the monomer frontier orbitals. They also applied this approach to triphenylamine dimer systems.[36]

The studies mentioned above deal with individual aspects of the calculation of transfer integrals, such as basis set convergence or the dependence on the exchange–correlation functional. To the present day, no systematic evaluation of the computational efficiency of the different approaches has been reported. This is in part due to the fact that the authors either

concentrated on simple model systems, like ethylene, or studied crystalline organic semiconductors, for instance the tetrathiafulvalene–tetracyanoquinodimethane (TTF–TCNQ) complex[34] or silole-based compounds,[35] with a limited number of unique molecular pairs due to crystal symmetry. However, for highly disordered systems like the prototypical Alq_3 this number can easily be in the order of 10^4 and the calculation of transfer integrals will be a serious bottleneck for the computation of charge carrier mobilities from either kinetic Monte-Carlo simulations or the solution of the Master equation. Therefore, it is vital to find a viable compromise between accuracy and timing of the calculations. In this context, the aim of this work is to complement the existing studies by analyzing the relation between the calculational parameters, like basis sets and model chemistry, and the associated computational costs for some representative cases. Thereby we want to derive an optimal set of parameters which will allow us to investigate charge transport mechanism in amorphous organic compounds based on multi-scale simulations with appropriate accuracy at manageable computational costs.

In order to be able to make a consistent comparison and explain the different steps of our discussion of several parameters, we will first recapitulate based on ref. 32 the general strategy for obtaining t_{nm}, ε_n, and ε_m between two neighboring molecules based on DFT calculations. We also pay special attention to its practical implementation which relies on the projection of molecular orbitals of monomers onto the manifold of the molecular orbitals of the dimer within a Counterpoise basis set.[37,38] In this paper, we refer to this method as DIPRO (short for dimer projection). After validating this strategy and its implementation using ethylene as a simple model system, we concentrate specifically on the evaluation of computational efficiency depending on the parameters of the underlying DFT calculations with the application to large-scale morphologies of disordered systems in mind. To this end, we pick representative parameters for the model chemistry, i.e. one standard hybrid (B3LYP) and one non-hybrid (PW91) exchange–correlation functional, as well as the MPW3LYP functional[39] that was introduced in application to weakly interacting systems. We use a Pople-style 6-311G basis set with and without polarization and diffusive extensions and compare the computational costs using sample pairs of Alq_3 (out of a large morphology) as a model system. We also consider various simplifications of the general DIPRO calculations, including a loosening of self-consistency requirements and the nature of the Counterpoise basis set.

This paper is organized as follows: In the first section, we will present the general methodology of determining intermolecular transfer integrals from quantum-chemistry calculations based on a projective method. The validity of this approach is first checked in section III using a simple model system consisting of two ethylene molecules. In order to assess the efficiency of the method upon changes to computational parameters such as basis sets, convergence criteria etc., we take one molecular pair out of a larger Alq_3 morphology and perform testing runs on this configuration. A brief summary concludes the paper.

II. Methodology

Here, we first recapitulate the findings of Valeev et al.,[32] while also paying special attention to the practical implementation of the method in the process. Let us write a version of eqn (2) for two molecules. We label the two individual molecules A and B and their frontier orbitals ϕ^A and ϕ^B, respectively. Throughout the paper we will consider the particular case of hole transport, where the frontier orbital of interest is the HOMO. All arguments can be applied to electron transfer by changing references to HOMOs to LUMOs. We now assume that the frontier orbitals of a dimer (adiabatic energy surfaces) result exclusively from the interaction of the frontier orbitals of monomers. In this approximation, they can be expanded in terms of ϕ^A and ϕ^B. The expansion coefficients, $\mathbf{C}$, can be determined by solving the generalized secular equation

$$(\underline{\mathbf{H}} - E\underline{\mathbf{S}})\mathbf{C} = 0, \tag{3}$$

where $\underline{\mathbf{H}}$ and $\underline{\mathbf{S}}$ are the Hamiltonian and overlap matrices of the system, respectively. They can be written explicitly as

$$\underline{\mathbf{H}} = \begin{pmatrix} e_A & J_{AB} \\ J_{AB} & e_B \end{pmatrix},$$

$$\underline{\mathbf{S}} = \begin{pmatrix} 1 & S_{AB} \\ S_{AB} & 1 \end{pmatrix}, \tag{4}$$

with

$$e_A = \langle \phi^A | \hat{H} | \phi^A \rangle,$$

$$e_B = \langle \phi^B | \hat{H} | \phi^B \rangle,$$

$$J_{AB} = \langle \phi^A | \hat{H} | \phi^B \rangle,$$

$$S_{AB} = \langle \phi^A | \phi^B \rangle. \tag{5}$$

It should already be stressed at this point that the two monomer HOMOs that form the basis of this expansion are not orthonormal in general, so that $\underline{\mathbf{S}} \neq \underline{\mathbf{1}}$. This is important when relating the e_m and J_{mn} to the site energies ε_m and transfer integrals t_{mn} defined in eqn (2), where an orthogonal basis set is assumed. Valeev et al.[32] have pointed out the significance of this in detail. Due to the non-orthonormality of the monomer HOMOs, the respective expressions are not identical. It is therefore necessary to suitably transform eqn (3) into a standard eigenvalue problem of the form

$$\underline{\mathbf{H}}^{\text{eff}}\mathbf{C} = E\mathbf{C}. \tag{6}$$

According to Löwdin[40] such a transformation can be achieved by multiplying the square-root of the inverted overlap matrix from the left and to the right to the Hamiltonian, i.e. by

$$\underline{\mathbf{H}}^{\text{eff}} = \underline{\mathbf{S}}^{-\frac{1}{2}}\underline{\mathbf{H}}\underline{\mathbf{S}}^{-\frac{1}{2}}. \tag{7}$$

Suzuki *et al.*[41] showed that $\underline{S}^{-\frac{1}{2}}$ can efficiently be calculated as

$$\underline{S}^{-\frac{1}{2}} = \underline{U}\underline{S}_0^{-\frac{1}{2}}\underline{U}^t = \underline{U}\begin{pmatrix} s_1 & & 0 \\ 0 & \ddots & 0 \\ 0 & & s_N \end{pmatrix}^{-\frac{1}{2}}\underline{U}^t$$

$$= \underline{U}\begin{pmatrix} s_1^{-\frac{1}{2}} & & 0 \\ 0 & \ddots & 0 \\ 0 & & s_N^{-\frac{1}{2}} \end{pmatrix}\underline{U}^t,$$

(8)

where the columns of the matrix $\underline{U}$ contain the N eigenvectors of the regular matrix $\underline{S}$, and $s_1,\ldots,s_N$ are the associated eigenvalues. Applying this procedure to the (2×2) case in eqn (3) then yields an effective Hamiltonian matrix in an orthonormalized basis, and its entries can directly be identified with the site energies ε_m and transfer integrals t_{mn} in eqn (2):

$$\underline{H}^{\text{eff}} = \begin{pmatrix} e_A^{\text{eff}} & J_{AB}^{\text{eff}} \\ J_{AB}^{\text{eff}} & e_B^{\text{eff}} \end{pmatrix} = \begin{pmatrix} \varepsilon_A & t_{AB} \\ t_{AB} & \varepsilon_B \end{pmatrix}.$$

(9)

Explicitly, the elements of the effective Hamilton matrix after application of eqn (7) read

$$e_{A(B)}^{\text{eff}} = \varepsilon_{A(B)}$$

$$= \frac{1}{2}\frac{1}{1-S_{AB}^2}\left((e_A + e_B) - 2J_{AB}S_{AB}(e_A - e_B)\sqrt{1-S_{AB}^2}\right)$$

$$J_{AB}^{\text{eff}} = t_{AB} = \frac{J_{AB} - \frac{1}{2}(e_A + e_B)S_{AB}}{1 - S_{AB}^2}.$$

(10)

It is apparent from eqn (10) that for orthogonal monomer HOMOs, *i.e.* when $S_{AB} = 0$, the modifications to $e_{A(B)}$ and J_{AB} vanish. In particular, this is the case for the commonly used ZINDO approach. In the approximation that the orbitals of the dimer ψ^D are determined only by the HOMOs of the monomers, the difference of the eigenvalues of the effective Hamiltonian in eqn (9), ΔE, is the value of the splitting between the HOMO and HOMO−1 levels of the dimer:

$$\Delta E = \sqrt{(\varepsilon_A - \varepsilon_B)^2 + (2t_{AB})^2}.$$

(11)

This indicates that the resulting energy split between HOMO and HOMO−1 in the dimer can in general not be attributed exclusively to the electronic coupling of the monomers represented by t_{AB} but can also affected by the difference in site energies, $\varepsilon_A - \varepsilon_B$. If one intends to determine the transfer integral t_{AB} from the dimer energy splitting, one must evaluate

$$t_{AB} = \frac{1}{2}\sqrt{(\Delta E)^2 - (\varepsilon_A - \varepsilon_B)^2}.$$

(12)

The difference of the site energies associated to the individual monomers in the dimer configuration is only zero when

the monomers are identical and their mutual geometric orientation can be generated by symmetry transformations that are compatible with the point group of the monomer, *i.e.* when the dimer is symmetric. In a non-symmetric dimer, monomer sites A and B polarize each other asymmetrically and consequently contribute differently to the energetics of the dimer. This also means that in general quantum-chemical information is needed from both monomers and the dimer to accurately determine the transfer integral.

Up to this point we have not mentioned in detail how to suitably calculate the matrix elements J_{AB}. Direct numerical integration in real space as in

$$J_{AB} = \langle\phi^A|\hat{H}|\phi^B\rangle = \int \phi^A(\mathbf{r})\hat{H}\phi^B(\mathbf{r})\,d^3r$$

(13)

is certainly very inefficient and potentially inaccurate. We can, however, be a little more resourceful. Let us consider the set of molecular orbitals for the dimer $\{\psi_i^D\}$. As eigenfunctions of the Hamiltonian operator of the dimer $\hat{H}$ they form a complete orthonormal system and the unity operator can be written as

$$\underline{1} = \sum_i |\psi_i\rangle\langle\psi_i|.$$

(14)

By inserting two unity operators into eqn (13) one finds that

$$J_{AB} = \left\langle \phi^A \sum_i |\psi_i\rangle\langle\psi_i|\hat{H}\sum_j |\psi_j\rangle\langle\psi_j|\phi^B \right\rangle$$

$$= \sum_i\sum_j \langle\phi^A|\psi_i\rangle\langle\psi_i|\hat{H}|\psi_j\rangle\langle\psi_j|\phi^B\rangle.$$

(15)

In the basis of its eigenfunctions $\{\psi_i\}$ the Hamiltonian operator $\hat{H}$ is diagonal with $\langle\psi_i|\hat{H}|\psi_j\rangle = \mathscr{E}_i\cdot\delta_{ij}$, where the $\mathscr{E}_i$ are the molecular orbital energies of the dimer. The terms $\gamma_i^A := \langle\phi^A|\psi_i\rangle$ and $\gamma_j^B := \langle\psi_j|\phi^B\rangle$ are the projections of the monomer orbitals ϕ^A and ϕ^B on the dimer orbitals ψ_i and ψ_j, respectively. With this the determination of J_{AB} reduces to

$$J_{AB} = \sum_i \gamma_i^A\mathscr{E}_i\gamma_i^B = \boldsymbol{\gamma}^A \cdot \text{diag}(\mathscr{E}_i)\boldsymbol{\gamma}^B.$$

(16)

What is left to do is determine these projections $\gamma_i^{A(B)}$. Again it is inconvenient to perform a real-space integration. In all practical calculations the molecular orbitals are expanded in basis sets of either plane waves or of localized atomic orbitals $\{\varphi_\alpha\}$. We will first consider the case that the calculations for the monomers are performed using a *counterpoise* (CP) basis set that is commonly used to deal with the basis set super-position error (BSSE).[37,38] The basis set of atom-centered orbitals of a monomer is extended to the one of the dimer by adding the respective atomic orbitals at virtual coordinates of the second monomer. We can then write the respective expansions as

$$|\phi^{A(B)}\rangle = \sum_\alpha \zeta_\alpha^{A(B)}|\varphi_\alpha\rangle,$$

$$|\psi_i\rangle = \sum_\alpha \zeta_\alpha^D|\varphi_\alpha\rangle.$$
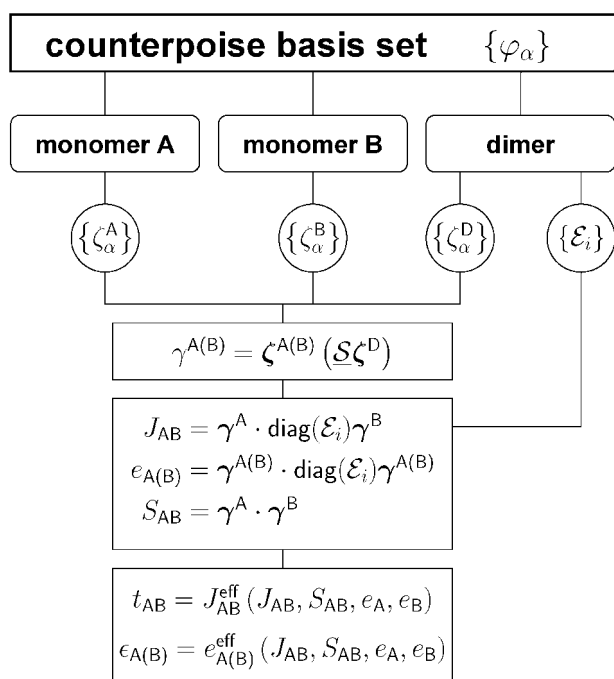
(17)

Fig. 1 Schematics of the DIPRO method.

The projections can then be determined within the common basis set:

$$
\begin{aligned}
\langle \phi^{A(B)} | \psi_i \rangle &= \sum_\alpha \zeta_\alpha^{A(B)} \langle \varphi_\alpha | \sum_\beta \zeta_\beta^D | \varphi_\beta \rangle \\
&= \sum_\alpha \sum_\beta \zeta_\alpha^{A(B)} \zeta_\beta^D \langle \varphi_\alpha | \varphi_\beta \rangle \\
&= \sum_\alpha \sum_\beta \zeta_\alpha^{A(B)} \mathscr{S}_{\alpha\beta} \zeta_\beta^D \\
&= \zeta^{A(B)} (\mathscr{S} \zeta^D),
\end{aligned}
\tag{18}
$$

where the $\mathscr{S}$ is the overlap matrix of the atomic orbitals.

We summarize this methodology, which we will from now on refer to as DIPRO, as the projection of monomer orbitals on dimer orbitals, by the schematics in Fig. 1. After completion of the quantum-chemical calculations for both monomers and dimers, the elements J_{AB} can be calculated using eqn (16) and (18) by simple matrix-vector (or matrix–matrix) multiplications. From a quantum-chemical calculation the overlap matrix of atomic orbitals $\mathscr{S}$, the expansion coefficients for monomer $\zeta_\alpha^{A(B)}$ and dimer orbitals ζ_α^D, as well as the orbital energies $\mathscr{E}_i$ of the dimer are required as input.

III. Results

In this section we will evaluate the efficiency of DIPRO using DFT calculations of different levels of sophistication in terms of employed basis sets, exchange–correlation functionals and self-consistency requirements with the specific application to large-scale morphologies of disordered systems in mind. To check the validity of the method and in particular its implementation we first consider a simple model system consisting of two ethylene molecules. Reference values from ZINDO

calculations using the Molecular Orbital Overlap (MOO) package[42] and also DFT results from the literature will be used to assess the accuracy of the procedure.

After that we gauge the efficiency using a more complicated model system. To this end, we take a pair of neighboring Alq$_3$ molecules out of a larger morphology obtained by molecular dynamics simulation[43] using the VOTCA package.[44] For this configuration we analyze the dependence of the calculated values for the transfer integrals and site-energies as well as the required computational costs on the choice of the parameters for the density-functional calculations.

All of the following calculations on the quantum-chemical level have been performed using the software package Gaussian 03[45] on eight processors of the IBM p575 Power5 system at MPG-RZG Garching. The evaluation of the transfer integrals and site-energies based on the output of these calculations is done with in-house code written in Python using cclib.[46]

A. Ethylene

As mentioned above, the first dimer configuration we consider is a co-facial orientation of two ethylene molecules (see inset of Fig. 2). As a first step, the geometry of a single molecule is optimized using the B3LYP hybrid-functional[47] and the 6-311++G(d,p) basis set, including diffuse and polarization functions. Based on this optimized geometry, we determine the transfer integral $|J_{AB}|$ for hole transport as a function of center-to-center distance d using both the ZINDO/MOO code and the DFT/DIPRO approach as given by eqn (10), for comparison.

The respective resulting transfer integrals are shown in Fig. 2. For the considered geometry, one can in general expect an exponential decay of the charge transfer parameter since the probability for charge hopping is mainly driven by the overlap of the HOMO orbitals of the monomers which decays exponentially with their mutual distance. This qualitative behavior is reflected in both the ZINDO and DFT results. In terms of absolute values, ZINDO/MOO and DFT/DIPRO approaches yield slightly different results. For small distances
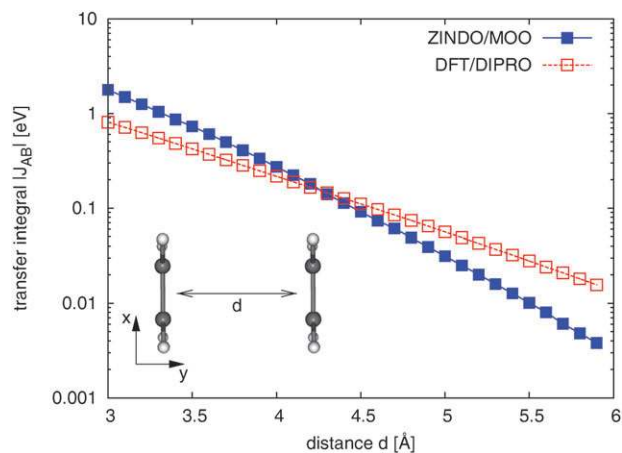

Fig. 2 Transfer integral $|J_{AB}|$ for hole transport (in eV) as a function of the displacement (in Å) between two C_2H_4 molecules in co-facial orientation as resulting from ZINDO-based (filled squares) and DFT-based (open squares) approaches, respectively.

between the monomers, the transfer integral determined by ZINDO is higher than that resulting from DFT. At the same time, it decays faster with increasing center-to-center distance and a crossover appears at about 4.3 Å. This appears to be a result of different orbital localizations in both approaches. By definition, the ZINDO basis set consists of more strongly localized functions. Hence, the overlap is high for small distances, while it also can account for the faster decay. Similar observations of the differences between the semi-empirical and *ab inito* methods have been made in ref. 33 and 42, for instance.

We note at this point that we also compared the results shown in Fig. 2 as obtained from eqn (10) to the respective energy level splits in the dimer. As was expected from eqn (12), both approaches yield identical transfer integrals for this symmetric dimer configuration, which further validates the implementation of the DIPRO method.

The fact that our DIPRO calculations are performed correctly is additionally supported by the comparison to results from literature. In ref. 32 Valeev *et al.* investigated the situation depicted in the inset of Fig. 3 in which the center-to-center distance between the two ethylene molecules is fixed at 5 Å. Then one of the monomers is rotated along its C=C double bond and the dependence of the transfer integral on the angle of rotation Ω is studied. The authors also employed DFT calculations on hybrid-functional level with only slightly different basis functions, allowing for a direct comparison to our DIPRO results. The results of the respective calculations are shown in Fig. 3. DFT/DIPRO results are indicated by open squares, while filled triangles represent data points taken from Fig. 1 of ref. 32. As reference, we also added ZINDO/ MOO results (filled squares). Clearly, the transfer integral is maximal for the co-facial orientation where the overlap between the π-orbitals is maximal and then gradually decreases to zero at an angle of 90°. In this face-to-edge orientation the π-orbitals of the two monomers are perpendicular and hence do not overlap. On a quantitative level, our DIPRO results and those from ref. 32 are in excellent

agreement. The transfer integrals from both DFT-based methods result higher than the respective ZINDO values, which is in accord with the findings in Fig. 2 for a distance of 5 Å.

From the above comparison, we can deduce that the DIPRO method as implemented allows for a reliably accurate DFT-based description of intermolecular transfer integrals.

B. Tris(8-hydroxyquinolinato)aluminium

While a simple molecule like ethylene is a suitable model system to study the basic functionality of the previously presented approach, it is not so convenient to investigate its computational cost and to evaluate its practical applicability to disordered systems of scientific interest, which are characterized by more complex molecules in large-scale morphologies. To investigate the charge-transport properties of such systems, *e.g.* based on Marcus theory for charge hopping in a kinetic Monte-Carlo simulation, it is essential that the required transfer integrals and site-energies are computed with satisfactory accuracy within a reasonable amount of time. For the quantum-chemical calculations in our DIPRO approach, several parameters for the DFT calculations significantly influence the quality of results and time required to obtain the results. Among those parameters are the choice of the basis set, the employed exchange–correlation functional, convergence criteria *etc*. In the following we will consider two sample pairs of Alq$_3$ taken from a larger morphology, as depicted in Fig. 4. Panel (a) shows a nearly ideal mutual orientation of the two molecules for hole transport.
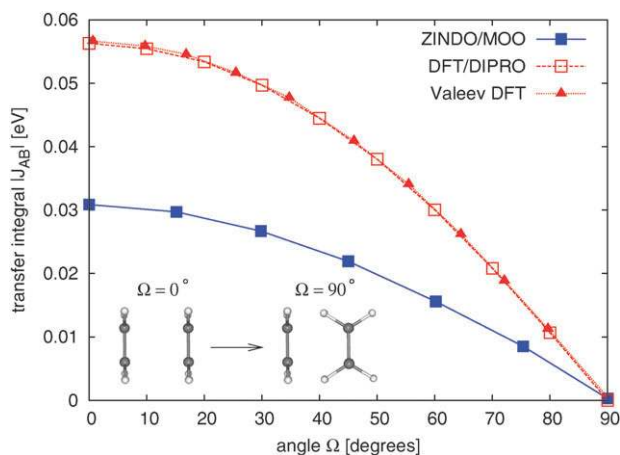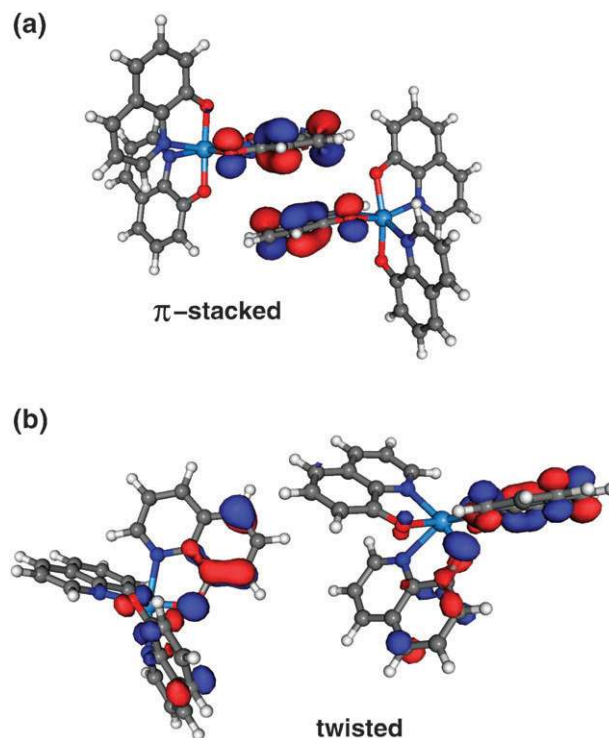

Fig. 3 Transfer integral $|J_{AB}|$ (in eV) as a function of rotation around the C=C double bond of one ethylene molecules as resulting from ZINDO (filled squares) and DFT-based approaches (DIPRO: open squares, ref. 32: filled triangles), respectively. The center-to-center distance of the two molecules is 5 Å.

Fig. 4 Two sample Alq$_3$ pairs taken out of a morphology containing 512 molecules. The upper panel (a) shows a nearly ideally π-stacked orientation, while the more common twisted configuration is depicted in panel (b). Isosurface representations of molecular HOMO densities have been added.

The respective arms of the molecules that host the HOMO are almost π-stacked, similar to the co-facial orientation of ethylene that we discussed in the preceding section. More common, however, is the configuration shown in Fig. 4(b), where the molecules are twisted against each other and also show a considerable amount of internal deformation. We will analyze how the computational parameters mentioned above affect the calculated transfer integrals and computational costs for these two cases. The latter we determine as the total run time T of the two-monomer and the one-dimer calculations on eight processors of the IBM p575 Power5 system at MPG-RZG Garching.

1. Basis sets. Let us first consider the results for hybrid-functional calculations for different levels of sophistication of the 6-311G basis set. We start with the 6-311++G(d,p) basis set, *i.e.* the most complete basis set including polarization [(d,p)] and diffuse [++] functions, and then gradually remove these from the basis set to assess their effect on the calculated properties. The respective results for the transfer integrals and site-energies of electrons and holes in the two sample configurations are listed in Table 1 (π-stacked) and Table 2 (twisted).

In the case of the π-stacked configuration, it is evident that the calculated transport parameters are fairly robust against changes in the basis set. Transfer integrals for holes are large, which is expected for this mutual arrangement of the two molecules. Even the simple 6-311G basis set already describes the transfer integrals and site-energies satisfactorily. Since the molecular orbitals, in particular the respective HOMOs, are strongly localized, they can be described in sufficient accuracy without additional basis functions. This is of great significance in terms of the computational costs listed in Table 1, from which it is obvious that the addition of polarization functions and in particular of diffuse functions increase the calculation times dramatically.

For the twisted configuration in Fig. 4(b), the situation is slightly different. The individual HOMOs show a more delocalized character compared to the π-stacked variant due to the twisting of the three arms of the Alq_3 molecules. Overall, the resulting hole transfer integrals listed in Table 2 (note that they are given in meV) are roughly one order of magnitude lower that in the above case. Since the states are less localized, the addition of more delocalized functions to the basis set becomes relevant. The dependence of the results for the twisted Alq_3 configuration on the basis sets is given in Table 2. Let us start with the case of the 6-311++G(d,p) basis set, *i.e.* the set containing both polarization and diffuse

Table 1 Dependence of the calculated transfer integrals and site-energies for the π-stacked Alq_3 pair for hole (h) and electron (e) transport on the choice of basis set for hybrid-functional DFT

B3LYP		J_{AB}^{eff} [eV]	e_A^{eff} [eV]	e_B^{eff} [eV]	T
6-311++G(d,p)	h	0.076	−4.79	−4.54	13 h 30 m
	e	0.255×10^{-3}	−2.45	−2.16	
6-311++G	h	0.077	−4.73	−4.47	7 h 00 m
	e	0.251×10^{-3}	−2.42	−2.15	
6-311G(d,p)	h	0.077	−4.73	−4.56	1 h 40 m
	e	0.203×10^{-3}	−2.23	−2.06	
6-311G	h	0.077	−4.62	−4.39	43 m
	e	0.291×10^{-3}	−2.31	−2.03	

Table 2 Dependence of the calculated transfer integrals and site-energies for the twisted Alq_3 pair for hole (h) and electron (e) transport on the choice of basis set for hybrid-functional DFT. Note that the J_{AB}^{eff} are given in meV, while ε_A^{eff} and ε_B^{eff} are in eV

B3LYP		J_{AB}^{eff} [meV]	e_B^{eff} [eV]	e_B^{eff} [eV]	T
6-311++G(d,p)	h	1.80	−5.47	−5.08	6 h 16 m
	e	2.52	−2.25	−2.38	
6-311++G	h	1.31	−5.49	−5.03	3 h 17 m
	e	2.31	−2.23	−2.36	
6-311G(d,p)	h	1.74	−5.36	−4.98	1 h 12 m
	e	2.39	−2.12	−2.25	
6-311G	h	1.20	−5.37	−4.95	35 m
	e	2.21	−2.13	−2.26	

functions, as a reference. Hole and electron transfer integrals are of the same order of magnitude so that the basis set analysis has to take both into account. The resulting transfer integral for holes is smaller by 0.49 meV after removal of the polarization functions (6-311++G) and smaller by 0.60 meV when also the polarization functions are not taken into account (6-311G). When only the diffuse functions are removed (6-311G(d,p)), the loss of accuracy is slight. Similar qualitative observations can be made for the electron transfer, so that the use of the 6-311G(d,p) basis set appears the most convenient in terms of accuracy. Unlike in the case of the π-stacked dimer, the simple 6-311G set cannot appropriately describe the charge transport properties.

2. Functionals. The use of a hybrid functional like B3LYP, which mixes Hartree–Fock exchange with a non-local DFT exchange–correlation functional, is in many cases more suitable to study properties of occupied and virtual molecular orbitals with high quantitative accuracy on an absolute scale, particularly with respect to single-particle transitions between the occupied and unoccupied manifolds. That said, it is also much more demanding computationally due to the explicit calculation of the Hartree–Fock exchange. Non-hybrid exchange–correlation functionals which only depend on the (local) charge density and its gradient are much less demanding but the resulting molecular properties show systematic errors, *e.g.* the underestimate of the HOMO–LUMO gap or the overestimation of energies of strongly-localized (correlated) electrons with d- or f-character.

Still, the use of a non-hybrid exchange–correlation functional such as PW91[48] as the basis of the DIPRO calculations of the transfer integrals is worth investigating, since only energy splittings within the occupied (hole transport) and unoccupied (electron transport) manifolds are relevant. This notion has also been studied, for instance by Huang and Kertesz,[33] who found only slight differences in the calculated transfer integrals for ethylene depending on the sophistication of the used functional. They compared calculated transfer integrals for TTF-TCNQ to experimental data and found slightly better agreement of results obtained from PW91 than from B3LYP. In this context, it is known that the hybrid-functional is often problematic to describe interactions in van der Waals and hydrogen-bonded systems.[49] For our investigation, we limit ourselves to the twisted dimer configuration which showed a higher dependence of the calculated transport

Table 3 Dependence of the calculated transfer integrals and site-energies for one Alq$_3$ pair for hole (h) and electron (e) transport on the choice of basis set for classical DFT using the PW91 functional. Note that the J_{AB}^{eff} are given in meV, while ε_A^{eff} and ε_B^{eff} are in eV

PW91		J_{AB}^{eff} [meV]	e_A^{eff} [eV]	e_B^{eff} [eV]	T
6-311++G(d,p)	h	1.26	−4.84	−4.50	3 h 01 m
	e	2.10	−2.90	−3.07	
6-311++G	h	0.87	−4.81	−4.42	1 h 35 m
	e	1.92	−2.88	−3.01	
6-311G(d,p)	h	1.47	−4.78	−4.41	40 m
	e	1.94	−2.74	−2.91	
6-311G	h	0.67	−4.68	−4.41	19 m
	e	1.91	−2.71	−2.93	

properties from the basis set before. Table 3 contains the relevant data for a calculation using the PW91 exchange–correlation functional analogous to the data listed in Table 2 in the case of B3LYP. On average, the transfer integrals resulting from PW91 are about 30% smaller than their respective B3LYP counterparts due to the lack of Hartree–Fock exchange. Similarly, the absolute values of the site-energies are smaller. However, their difference, $e_A^{eff} - e_B^{eff}$, is hardly affected by the change in functional. With respect to the basis set dependence, the conclusions hold that have been drawn in the case of the hybrid-functional calculations. The slight reduction of the value of the transfer integrals is paralleled by a substantial reduction in computational costs. In this case, the non-hybrid DFT simulation is faster by about a factor of two. For more localized charge distributions, as in the π-stacked case, this can even be a factor of three due to the more localized states and the inherently more elaborate evaluation of the Hartree–Fock exchange.

We have also tested the use of the MPW3LYP functional[39] that is, along with other similarly modified functionals, considered more appropriate for application to non-covalently bonded systems. The respective results are summarized in Table 4, and the comparison to the results from standard B3LYP calculations in Table 2 indicates negligible effects on the determined transfer integrals and site-energies.

As can be seen from Tables 2–4, the computational cost T for calculating transport properties based on DFT – roughly in the order of one to two hours – is still substantial. This is particularly critical, since a realistic morphology typically consists of several thousands of individual molecules and a respectively large number of neighbor pairs N_p for which the

transfer integrals and site-energies are required. The total computational costs than can be estimated to amount to $T_{tot} = N_p T$. It is evident that the applicability of the DIPRO approach as it is presented above is limited to small morphologies and only very specific cases.

3. Convergence criteria. Up to this point, we have studied the effects of basis sets and exchange–correlation functionals on the calculated charge transport properties. All calculations were performed under the tacit assumption that we require full convergence for the individual monomer and dimer configurations.

In practical calculations, it might be considerable to loosen the convergence criteria and save computer time in the process. The default criterion used by Gaussian 03 is that the root-mean-square (RMS) density matrix is smaller that 10^{-4}. For higher RMS values the respective calculations will need fewer cycles to reach self-consistency. We repeated the calculations on the 6-311G(d,p)/B3LYP level[50] for RMS values of 10^{-3}, 10^{-2} and 10^{-1}, and list the results in Table 5. We find that the resulting transfer integrals and site-energies are relatively robust when a RMS density of 10^{-3} is used as convergence criterion instead of the default. Concomitantly, the computation time is reduced to about three-quarters of the previous value. Further loosening of the convergence requirements only reduces the computation times marginally, while accuracy is lost. In the case of a RMS density of 10^{-2} the transfer integrals for holes and electrons are still within acceptable limits. Site-energies, however, are more strongly affected so that the energetic disorder in ΔG_{AB} in eqn (1) will be inaccurate.

Another possible simplification of the DIPRO approach is motivated by the following: First of all, we determine the molecular orbitals of the monomers $\{\phi_j^A\}$ and $\{\phi_k^B\}$ self-consistently, as usual. Since the dimer is a combined configuration of these two monomers, one can construct an initial guess for the manifold of occupied molecular orbitals of the dimer $\{\psi_i^D\}_{occ}^{(0)}$ as a superposition of the respective occupied manifolds of the monomers, i.e.

$$\{\psi_i^D\}_{occ}^{(0)} = \{\phi_j^A\}_{occ} \oplus \{\phi_k^B\}_{occ}. \quad (19)$$

As long as inter-molecular interactions are weak in the dimer configuration, one can assume that the self-consistent ground-state of the dimer is well approximated by this initial guess. The practical idea is therefore to supply the superposition of

Table 4 Dependence of the calculated transfer integrals and site-energies for one Alq$_3$ pair for hole (h) and electron (e) transport on the choice of basis set using the MPW3LYP functional. Note that the J_{AB}^{eff} are given in meV, while ε_A^{eff} and ε_B^{eff} are in eV

MPW3LYP		J_{AB}^{eff} [meV]	e_A^{eff} [eV]	e_B^{eff} [eV]	T
6-311++G(d,p)	h	1.81	−5.50	−5.11	8 h 06 m
	e	2.45	−2.29	−2.41	
6-311++G	h	1.32	−5.49	−5.06	3 h 55 m
	e	2.24	−2.26	−2.40	
6-311G(d,p)	h	1.72	−5.38	−5.00	1 h 13 m
	e	2.40	−2.14	−2.27	
6-311G	h	1.20	−5.39	−4.97	30 m
	e	2.21	−2.15	−2.29	

Table 5 Dependence of the calculated transfer integrals and site-energies for one Alq$_3$ pair for hole (h) and electron (e) transport on the convergence criterion for hybrid DFT using the B3LYP functional and the 6-311G(d,p) basis set. Note that the J_{AB}^{eff} are given in meV, while ε_A^{eff} and ε_B^{eff} are in eV

6-311G(d,p)/B3LYP		J_{AB}^{eff} [meV]	e_A^{eff} [eV]	e_B^{eff} [eV]	T
RMS density $< 10^{-4}$	h	1.74	−5.36	−4.98	1 h 12 m
	e	2.39	−2.12	−2.25	
RMS density $< 10^{-3}$	h	1.67	−5.39	−4.97	53 m
	e	2.36	−2.12	−2.23	
RMS density $< 10^{-2}$	h	1.63	−5.38	−5.17	50 m
	e	2.16	−2.28	−2.48	
RMS density $< 10^{-1}$	h	1.84	−5.44	−4.71	40 m
	e	2.56	−2.38	−2.46	

Table 6 Dependence of the calculated transfer integrals and site-energies for one Alq_3 pair for hole (h) and electron (e) transport on the dimer calculation mode (SCF or noSCF) for hybrid DFT using the B3LYP functional and the 6-311G(d,p) basis set. The RMS densities of the monomers are converged to 10^{-4} and 10^{-3}, respectively. Note that the J_{AB}^{eff} are given in meV, while ε_A^{eff} and ε_B^{eff} are in eV

6-311G(d,p)/B3LYP		J_{AB}^{eff} [meV]	e_A^{eff} [eV]	e_B^{eff} [eV]	T
RMS density $< 10^{-4}$					
SCF	h	1.74	-5.36	-4.98	1 h 12 m
	e	2.39	-2.12	-2.25	
noSCF	h	1.70	-5.36	-4.99	50 m
	e	2.31	-2.10	-2.26	
RMS density $< 10^{-3}$					
SCF	h	1.67	-5.39	-4.97	53 m
	e	2.36	-2.12	-2.23	
noSCF	h	1.78	-5.21	-4.65	38 m
	e	2.46	-2.00	-1.93	

occupied monomer manifolds as initial guess for the occupied dimer orbitals, set up the Fock matrix with $H_{ij}^{(0)} = \langle \psi_i^{(0)} | \hat{H} | \psi_j^{(0)} \rangle$ and solve the generalized secular equation. After this single iteration step, the dimer molecular orbitals $\{\psi_i^D\}^{(1)}$ and their energies $\{\mathscr{E}_i\}^{(1)}$ are printed out. This variant will be referred to as noSCF in the following, while we will label the standard procedure with a fully self-consistently converged dimer calculation as SCF, for the sake of clarity. The noSCF approach is closely related to the approach used in ref. 35 and 36. In Table 6 we summarize the results of noSCF DIPRO calculations based on a RMS density convergence for the monomers of 10^{-4} and 10^{-3}, respectively. For easier comparison, we also repeat the respective results of the standard calculations (referred to as SCF) from Table 5. It is obvious from the given transfer integrals and site-energies that the noSCF variant of the DIPRO calculation yields transport properties in very good agreement with the respective results from SCF calculation for the standard RMS density convergence criterion of 10^{-4} for the monomers. For a criterion of 10^{-3}, in contrast, the deviations of the calculated transfer integrals are slightly larger, and again, it is the site-energies that are affected more strongly. It is particularly noteworthy that in case of electron transport the site-energy difference changes sign, which would lead to significant modifications in the calculated transport rates. From the results, it can be concluded that a noSCF DIPRO calculation is only reliable if the convergence of the monomer orbitals is appropriate. In the case of the Alq_3 molecule, a noSCF calculations saves about 30% of computation time compared to a SCF run. Of the 50 min computation time per pair using the default convergence criterion, only seven minutes (or about 15%) are attributed to the noSCF dimer calculation. Any further significant reduction in computation time must therefore be achieved concentrating on the monomer calculations.

4. Abandoning the counterpoise basis set. In all previous calculations for the monomers, the use of a counterpoise basis set was assumed explicitly. This extension of the purely atom-centered molecular basis set is in principle more exact; however, it also increases the computational costs significantly. Also, since in the kind of morphologies we are interested in the average distances between the individual

molecules are not excessively small, the effect on the calculated molecular orbitals is expected to be slight. It is also known from the literature that the BSSE is critical mainly for total energies and less so for molecular orbitals and their single-particle energies. We therefore investigate also the case in which the monomer calculations are performed without additional ghost atoms located at the virtual positions of the second monomer. In this case the dimer basis set is the direct sum of the two monomer bases $\{\varphi_\alpha^D\} = \{\varphi_\beta^A\} \oplus \{\varphi_\gamma^B\}$. To evaluate the transfer integrals and site-energies using this noCP variant of the DIPRO method, we can hence rely on eqn (16) and (18) as long as we add an appropriate number of zeros to $\zeta^{A(B)}$ accounting for the differences in basis-sets. A schematic that illustrates the combination of the noCP and noSCF simplifications to the DIPRO method discussed above is given in Fig. 5.

To assess the accuracy and efficiency of the noCP basis, we again consider the two RMS density convergence criteria 10^{-4} and 10^{-3} and compare the results of noCP DIPRO calculations to the standard ones. At the same time, we also analyze the combination of noCP and noSCF in Table 7. For the standard density criterion, we find that both noCP and noCP + noSCF methods agree well with the results obtained using the counterpoise basis. The computation time can be reduced to as little as only 23 min, or 30% of the original value. For the convergence criterion 10^{-3} we note very similar behavior. Just as when using the counterpoise basis, a noSCF calculation with this criterion results in an inconsistent description of the site-energies in the case of electron transport.

5. Conclusions. To summarize the findings of the discussion on the accuracy and efficiency of the different variants of the DIPRO method, we show in Fig. 6 a comparison of average runtimes $\bar{T}$ estimated for a larger morphology, calculated transfer integrals, as well as site-energies, referenced to the respective values obtained using the general CP + SCF method. The use of the noCP variant of the DIPRO approach is even more advisable for large-scale simulations than the discussion on single pairs might indicate. Since the monomer calculations are no longer coupled for each dimer configuration due to the counterpoise basis, only one single DFT calculation has to be performed for each individual molecule in the morphology. This can be done before the dimer calculations are started. When N_m and N_d are the number of molecules and dimer pairs in the morphology, respectively, estimates for the total computation time of the four variants are

$$T^{CP,i} = N_d(2T_m^{CP} + T_d^i)$$
$$T^{noCP,i} = N_m T_m^{noCP} + N_d T_d^i, \quad (20)$$

where i can be either SCF or noSCF. If we assume an average number of unique neighbors per molecule, i.e. $N_b = \kappa N_m$, we can write the average time per dimer $\bar{T} = T/N_d$ as

$$\bar{T}^{CP,i} = 2T_m^{CP} + T_d^i$$
$$\bar{T}^{noCP,i} = \frac{T_m^{noCP}}{\kappa} + T_d^i \quad (21)$$
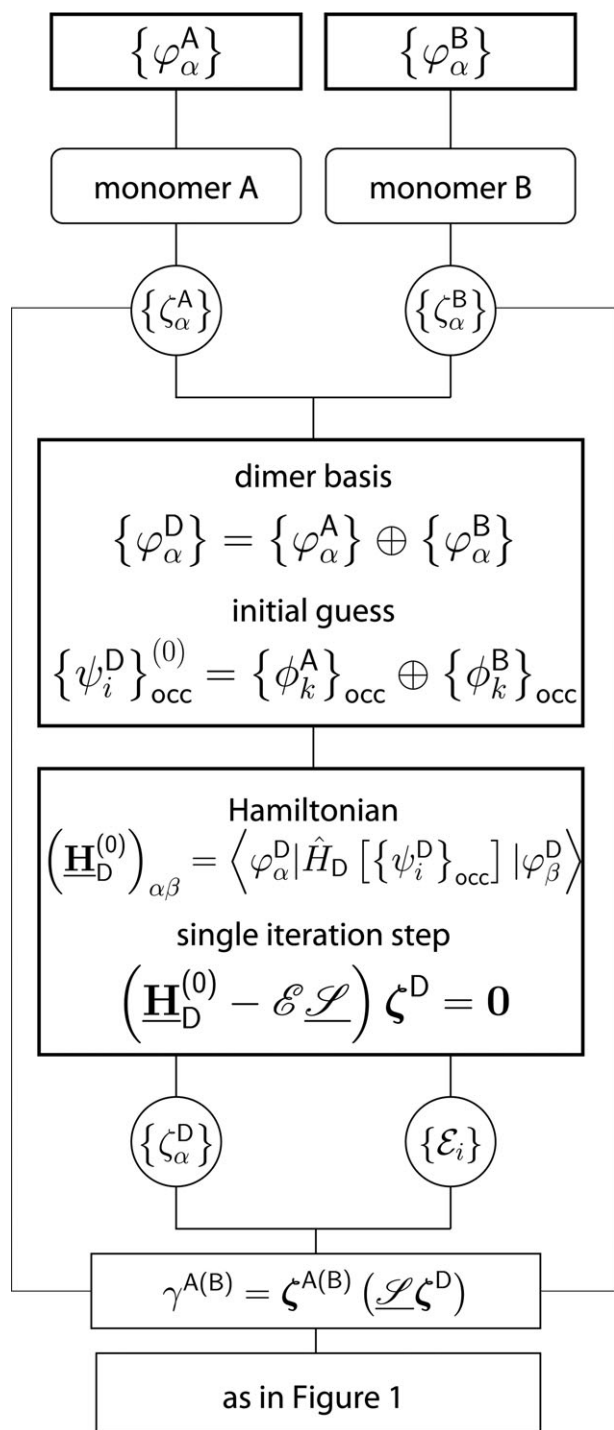
Fig. 5 Schematics of the noCP + noSCF variant of the DIPRO method. In this variant the monomer calculations can be performed independently from their mutual orientations in the dimer configurations.

In our sample morphology we have 512 molecules with 3046 unique neighbor pairs, so that there are six dimers per molecule on average. The determination of the transport properties for this morphology would then require total (average) computation times of ~ 155 days (72 min) in the SCF variant or ~ 108 days (50 min) in the noSCF variant using the counterpoise basis. In the noCP mode, the times

Table 7 Dependence of the calculated transfer integrals and site-energies for one Alq_3 pair for hole (h) and electron (e) transport on the basis set choice (CP or noCP) for hybrid DFT using the B3LYP functional and the 6-311G(d,p) basis set. The RMS densities are converged to 10^{-4} and 10^{-3}, respectively. Note that the J_{AB}^{eff} are given in meV, while ε_A^{eff} and ε_B^{eff} are in eV

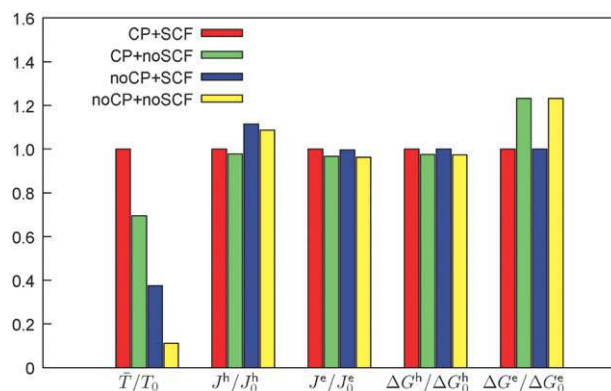| 6-311G(d,p)/B3LYP		J_{AB}^{eff} [meV]	e_A^{eff} [eV]	e_B^{eff} [eV]	T
RMS density < 10^{-4}					
CP	h	1.74	−5.36	−4.98	1 h 12 m
	e	2.39	−2.12	−2.25	
noCP	h	1.94	−5.36	−4.98	45 m
	e	2.38	−2.12	−2.25	
noCP + noSCF	h	1.89	−5.36	−4.99	23 m
	e	2.30	−2.10	−2.26	
RMS density < 10^{-3}					
CP	h	1.67	−5.39	−4.97	53 m
	e	2.36	−2.12	−2.23	
noCP	h	1.84	−5.39	−4.97	33 m
	e	2.30	−2.17	−2.23	
noCP + noSCF	h	1.92	−5.21	−4.64	18 m
	e	2.32	−2.00	−1.92	

Fig. 6 Comparison of the development of average computational cost $\bar{T}$, transfer integrals, and site-energies, referred to the values associated to the CP + SCF variant of the DIPRO method. Results are shown for the standard convergence criterion.

are ~ 64 days (27 min) and ~ 18 days (8 min) for SCF and noSCF, respectively. Since the use of noCP + noSCF does not result in any significant loss of accuracy, we conclude that this is the variant recommended for studies of charge transport in large-scale morphologies of amorphous organic compounds.

IV. Summary

In this work we have presented a projective method to determine intermolecular transfer integrals and site-energies required for the calculation of Marcus rates based on density-functional calculations. The accuracy and efficiency of this method depending on computational parameters such as basis sets, exchange–correlation functionals, and convergence criteria, has been investigated in detail in order to establish a suitable strategy for the simulation of charge transport in large morphologies. Using sample pairs of tris(8-hydroxyquinolinato)aluminium, we found that adding polarization functions to the 6-311G basis set is required to obtain reliable results. We recommend to use only the atom-centered basis set (noCP) for monomer and dimer

calculations in combination with the noSCF simplification for the dimer geometry as the most reasonable compromise between accuracy and computational costs. The use of PW91 instead of B3LYP on average reduces computation times by 30–40%, with transfer integrals also being systematically smaller by that percentage. Without experimental data, no preference for either functional can be made *a priori*.

Acknowledgements

References and notes

1 V. Lemaur *et al.*, *J. Am. Chem. Soc.*, 2004, **126**, 3271.
2 V. Coropceanu, J. Cornil, D. A. da Silva Filho, Y. Olivier, R. Silbey and J.-L. Bredas, *Chem. Rev.*, 2007, **107**, 926.
3 X. Feng, V. Marcon, W. Pisula, M. Hansen, J. Kirkpatrick, F. Grozema, D. Andrienko, K. Kremer and K. Müllen, *Nat. Mater.*, 2009, **8**, 421.
4 J. Nelson, J. Kwiatkowski, J. Kirkpatrick and J. Frost, *Acc. Chem. Res.*, 2009, **42**, 1768.
5 V. Marcon, D. Breiby, W. Pisula, J. Dahl, J. Kirkpatrick, S. Patwardhan, F. Grozema and D. Andrienko, *J. Am. Chem. Soc.*, 2009, **131**, 11426.
6 Y. Cheng, R. Silbey, D. da Silva, J. Calbert, J. Cornil and J. Bredas, *J. Chem. Phys.*, 2003, **118**, 3764.
7 G. R. Hutchison, Y.-J. Zhao, B. Delley, A. J. Freeman, M. A. Ratner and T. J. Marks, *Phys. Rev. B: Condens. Matter Mater. Phys.*, 2003, **68**, 035204.
8 E.-G. Kim, V. Coropceanu, N. Gruhn, R. Sánchez-Carrera, R. Snoeberger, A. Matzger and J.-L. Brédas, *J. Am. Chem. Soc.*, 2007, **129**, 13072.
9 O. Ostroverkhova, D. G. Cooke, F. A. Hegmann, J. E. Anthony, V. Podzorov, M. E. Gershenson, O. D. Jurchescu and T. T. M. Palstra, *Appl. Phys. Lett.*, 2006, **88**, 162101.
10 R. W. Munn and R. Silbey, *J. Chem. Phys.*, 1985, **83**, 1843.
11 R. W. Munn and R. Silbey, *J. Chem. Phys.*, 1985, **83**, 1854.
12 K. Hannewald and P. A. Bobbert, *Appl. Phys. Lett.*, 2004, **85**, 1535.
13 K. Hannewald and P. A. Bobbert, *Phys. Rev. B: Condens. Matter Mater. Phys.*, 2004, **69**, 075212.
14 A. Troisi and G. Orlandi, *Phys. Rev. Lett.*, 2006, **96**, 086601.
15 A. Troisi, *Adv. Mater.*, 2007, **19**, 2000.
16 D. L. Cheung and A. Troisi, *Phys. Chem. Chem. Phys.*, 2008, **10**, 5941.
17 P. M. Borsenberger, L. Pautmeier and H. Bassler, *J. Chem. Phys.*, 1991, **94**, 5447.
18 R. A. Marcus, *Rev. Mod. Phys.*, 1993, **65**, 599.
19 G. R. Hutchison, M. A. Ratner and T. J. Marks, *J. Am. Chem. Soc.*, 2005, **127**, 2339.
20 D. Andrienko, J. Kirkpatrick, V. Marcon, J. Nelson and K. Kremer, *Phys. Status Solidi B*, 2008, **245**, 830.
21 J. Kirkpatrick, V. Marcon, J. Nelson and D. Andrienko, *Phys. Status Solidi B*, 2008, **245**, 835.
22 V. Marcon, J. Kirkpatrick, W. Pisula and D. Andrienko, *Phys. Status Solidi B*, 2008, **245**, 820.
23 V. Rühle, J. Kirkpatrick and D. Andrienko, *J. Chem. Phys.*, 2010, **132**, 134103.
24 Y. Olivier, L. Muccioli, V. Lemaur, Y. Geerts, C. Zannoni and J. Cornil, *J. Phys. Chem. B*, 2009, **113**, 14102.
25 Z. G. Yu, D. L. Smith, A. Saxena, R. L. Martin and A. R. Bishop, *Phys. Rev. Lett.*, 2000, **84**, 721.
26 P. M. Borsenberger and M. B. O'Regan, *Chem. Phys.*, 1995, **200**, 257.
27 J. J. Kwiatkowski, J. Nelson, H. Li, J. L. Bredas, W. Wenzel and C. Lennartz, *Phys. Chem. Chem. Phys.*, 2008, **10**, 1852.
28 Y. Nagata and C. Lennartz, *J. Chem. Phys.*, 2008, **129**, 034709.
29 J. Kirkpatrick, V. Marcon, K. Kremer, J. Nelson and D. Andrienko, *J. Chem. Phys.*, 2008, **129**, 094506.
30 S. Naka, H. Okada, H. Onnagawa, Y. Yamaguchi and T. Tsutsui, *Synth. Met.*, 2000, **111–112**, 331.
31 W. Brütting, *Physics of Organic Semiconductors*, Wiley-VCH, Berlin, 2005, pp. 95–126.
32 E. F. Valeev, D. A. d. S. F. V. Coropceanu, S. Salman and J.-L. Brèdas, *J. Am. Chem. Soc.*, 2006, **128**, 9882.
33 J. Huang and M. Kertesz, *J. Chem. Phys.*, 2005, **122**, 234707.
34 J. Huang and M. Kertesz, *Chem. Phys. Lett.*, 2004, **390**, 110.
35 S. Yin, Y. Yi, Q. Li, G. Yu, Y. Liu and Z. Shuai, *J. Phys. Chem. A*, 2006, **110**, 7138.
36 X. Yang, Q. Li and Z. Shuai, *Nanotechnology*, 2007, **18**, 424029.
37 S. Boys and F. Bernardi, *Mol. Phys.*, 1970, **19**, 553.
38 S. Simon, M. Duran and J. J. Dannenberg, *J. Chem. Phys.*, 1996, **105**, 11024.
39 Y. Zhao and D. G. Truhlar, *J. Phys. Chem. A*, 2004, **108**, 6908.
40 P.-O. Löwdin, *J. Chem. Phys.*, 1950, **18**, 365.
41 K. Suzuki, S. Maruyama and K. Araki, *Bull. Chem. Soc. Jpn.*, 1973, **46**, 355.
42 J. Kirkpatrick, *Int. J. Quantum Chem.*, 2008, **108**, 51.
43 A. Lukyanov, C. Lennartz and D. Andrienko, *Phys. Status Solidi A*, 2009, **206**, 2737.
44 V. Rühle, C. Junghans, A. Lukyanov, K. Kremer and D. Andrienko, *J. Chem. Theory Comput.*, 2009, **5**, 3211.
45 M. J. Frisch *et al.*, *GAUSSIAN 03 (Revision C.02)*, Gaussian, Inc, Wallingford, CT, 2004.
46 N. M. O'Boyle, A. L. Tenderholt and K. M. Langner, *J. Comput. Chem.*, 2008, **29**, 839.
47 A. D. Becke, *J. Chem. Phys.*, 1993, **98**, 5648.
48 J. P. Perdew, in *Electronic Structure of Solids*, ed. P. Ziesche and H. Eschrig, Akademie Verlag, Berlin, 1991, p. 11.
49 S. Tsuzuki and H. P. Lüthi, *J. Chem. Phys.*, 2001, **114**, 3949.
50 We use B3LYP for the remainder of the paper as it better allows us to define an upper limit for the computational cost T. This does not constitute any preference of this level of theory over non-hybrid functionals for the systems under study.